**The EMBO Journal (2009) 28,** 3623–3632 | © 2009 European Molecular Biology Organization | All Rights Reserved 0261-4189/09
www.embojournal.org

THE EMBO JOURNAL

# The structure of an integrin/talin complex reveals the basis of inside-out signal transduction

**Nicholas J Anthis[1,4,*], Kate L Wegener[1], Feng Ye[2], Chungho Kim[2], Benjamin T Goult[3], Edward D Lowe[1], Ioannis Vakonakis[1], Neil Bate[3], David R Critchley[3], Mark H Ginsberg[2] and Iain D Campbell[1,*]**

[1]Department of Biochemistry, University of Oxford, Oxford, UK, [2]Department of Medicine, University of California San Diego, La Jolla, CA, USA and [3]Department of Biochemistry, University of Leicester, Leicester, UK

**Fundamental to cell adhesion and migration, integrins are large heterodimeric membrane proteins that uniquely mediate inside-out signal transduction, whereby adhesion to the extracellular matrix is activated from within the cell by direct binding of talin to the cytoplasmic tail of the β integrin subunit. Here, we report the first structure of talin bound to an authentic full-length β integrin tail. Using biophysical and whole cell measurements, we show that a specific ionic interaction between the talin F3 domain and the membrane–proximal helix of the β tail disrupts an integrin α/β salt bridge that helps maintain the integrin inactive state. Second, we identify a positively charged surface on the talin F2 domain that precisely orients talin to disrupt the heterodimeric integrin transmembrane (TM) complex. These results show key structural features that explain the ability of talin to mediate inside-out TM signalling.**

*The EMBO Journal* (2009) **28,** 3623–3632. doi:10.1038/emboj.2009.287; Published online 1 October 2009
*Subject Categories*: signal transduction; structural biology
*Keywords*: cell adhesion; crystallography; integrin activation; NMR; talin

## Introduction

Integrins are essential to biological functions that range from leukocyte trafficking to tissue integrity; these adhesion receptors are also therapeutic targets in thrombosis, inflammation, and cancer. Each α and β subunit of the integrin heterodimer consists of several linked globular extracellular domains, a single transmembrane (TM) helix, and a generally short cytoplasmic tail. Cellular modulation of integrin affinity ('activation') has a pivotal role in the biological function of these receptors and is the subject of much current interest (Hynes, 2002; Calderwood, 2004; Campbell and Ginsberg, 2004; Ginsberg *et al*, 2005). There is some controversy about the exact structure of the high- and low-affinity states, but strong evidence indicates that activation is initiated by protein–protein interactions with the cytoplasmic domains, causing tail separation and propagation of conformational changes to the outside of the cell (Lu *et al*, 2001; Takagi *et al*, 2001; Kim *et al*, 2003; Partridge *et al*, 2005; Arnaout *et al*, 2007; Luo *et al*, 2007; Wegener and Campbell, 2008; Askari *et al*, 2009). A key event is binding to the integrin β cytoplasmic tail by talin (Tadokoro *et al*, 2003; Nieswandt *et al*, 2007; Petrich *et al*, 2007a, b), a 270 kDa protein (capable of forming homodimers) with an N-terminal head domain (comprising F0, F1, F2, and F3 subdomains) and a C-terminal rod domain that binds to vinculin and actin (Critchley and Gingras, 2008) (Figure 1C). Binding of the F3 domain to integrin β tails is sufficient for integrin activation (Calderwood *et al*, 2002), although other head domains contribute to activation (Bouaouina *et al*, 2008).

Structural studies of integrin activation have been hampered by the weak nature of the talin/integrin interaction. Various strategies have been used to overcome this problem, beginning with a crystal structure of a short membrane–distal fragment of the β3 tail covalently tethered to the talin1 F2–F3 fragment (Garcia-Alvarez *et al*, 2003). This showed that the F3 domain interacts with the NPxY motif of the β3 tail in canonical PTB domain fashion (Calderwood *et al*, 2003), but this gave no information about the membrane–proximal region of the β3 tail, a region known to be essential for activation (Hughes *et al*, 1995; Vinogradova *et al*, 2002; Ulmer *et al*, 2003). A second structure, solved by NMR, elucidated the interface between the F3 domain and the β3 membrane–proximal helix (Wegener *et al*, 2007). This was made possible by constructing a chimaeric peptide of the β3 helix attached to a sequence from PIPK1γ that binds tightly to the talin NPxY binding pocket (Barsukov *et al*, 2003; de Pereda *et al*, 2005). These studies offered some insight into the β3/talin1 complex and the structural basis of integrin activation.

Prior structural studies of integrin activation by talin have involved a single integrin and talin isoform. However, mammals express two isoforms of talin (Figure 1B) and eight different β integrins, some of which exhibit additional splice variants (Figure 1A). In this study, we explore a wider range of talin/integrin interactions to identify a pair more suitable for structure determination. The resulting crystal structure, along with a multifaceted experimental approach, reveals a concerted series of evolutionarily conserved interactions that initiate inside-out signalling.

## Results

### *The structure of the talin2/β1D complex*

Through NMR studies of β tail/talin complexes (Table I; Supplementary Figure S1) we found that integrin β tails differ

*Corresponding authors. NJ Anthis or ID Campbell, Department of Biochemistry, University of Oxford, South Parks Road, Oxford OX1 3QU, UK. Tel.: +44 1865 613 200; Fax: +44 1865 613 201;
E-mail: nick.anthis@gmail.com or iain.campbell@bioch.ox.ac.uk
[4]Present address: Laboratory of Chemical Physics, Building 5, National Institute of Diabetes and Digestive and Kidney Diseases, National Institutes of Health, Bethesda, MD 20892-0520, USA

**Received: 1 August 2009; accepted: 3 September 2009; published online: 1 October 2009**

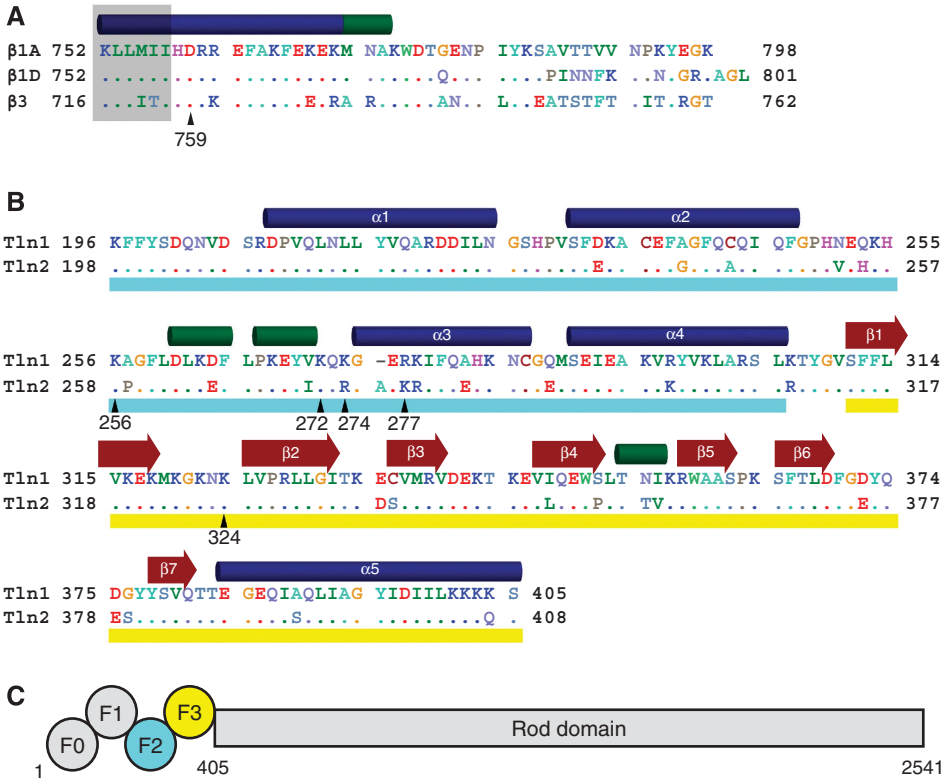


**Figure 1** Integrin and talin sequence comparisons. (**A**) Sequence of the cytoplasmic tail of the β1A, β1D, and β3 integrins. Residues in β1D and β3 that differ from β1A are highlighted, and a key membrane–proximal aspartate residue is indicated with β1 numbering. Secondary structure (α helices in blue, $3_{10}$ helices in green) is based on the β1D/talin2 complex structure. Residues embedded in the membrane (Lau *et al*, 2008b) are shaded in grey. Residues are coloured by chemical properties: acidic residues are shown in red, basic in blue, aliphatic in green, aromatic in cyan, polar in lavender, and others are given unique colouring. (**B**) Sequence of the F2–F3 domains of talin1 and talin2. Residues in talin2 that differ from talin1 are highlighted, and secondary structure was determined as in (A). The F2 domain is underlined in cyan and the F3 in yellow. (**C**) A schematic of the domain structure of talin. Talin homodimerization (not shown) occurs at the C-terminus.

**Table I** $K_d$ values of talin F3/β integrin tail interactions

| | Talin1 | Talin2 |
|---|---|---|
| β1A | 490 ± 10 | 652 ± 20 |
| β1D | 95 ± 4 | 36 ± 2 |
| β3 | 273 ± 6 | 438 ± 15 |

$K_d$ values are given in μM ± s.e.

widely in their affinity for different isoforms of talin and that β1D binds to talin2 with a much higher affinity than any previously studied integrin/talin pair. Talin2 and β1D, a splice variant of β1 differing from β1A only in its C-terminus (Figure 1A), are the major isoforms found in striated muscle (Belkin *et al*, 1996; Senetar *et al*, 2007; Conti *et al*, 2008), and the formation of this higher affinity complex is consistent with the high forces that this talin/integrin complex is subjected to in myotendinous junctions (Belkin *et al*, 1996; Conti *et al*, 2008).

This tighter complex crystallized, thus enabling us to solve the structure of the β1D integrin tail/talin2 F2–F3 complex at 2.2 Å resolution (Figure 2A; Table II). This is the first structure of talin bound to an authentic β integrin tail and the first involving either of these two striated muscle-specific isoforms. Each asymmetric unit in the crystal contained two integrin/talin heterodimers (Supplementary Figure S2A) with distinct electron density visible for the N-terminal 37 residues of the integrin tail (Supplementary Figure S3). The last 13 residues were not observed, suggesting that they remain unstructured. The talin2 F2–F3 domains exhibit similar folds and relative orientations to those seen in previous talin1 F2–F3 structures (Supplementary Figure S2B; Supplementary Table I), and the interface of the membrane–proximal integrin helix with the talin F3 activation loop is similar to that observed for the β3/PIPK1γ chimaera (Supplementary Figure S2C). This new structure allows detailed comparisons of the complexes formed between different talin and integrin isoforms; further analysis to define the structural basis of differing integrin/talin affinities—focusing on the more membrane–distal portions of this interface—will be an important area of future study. However, here we show that the β1D integrin tail/talin2 F2–F3 structure also reveals several novel features that permit the formulation of a new comprehensive structural model of integrin activation.

### *A positively charged patch on the talin F2 domain binds to the cell membrane*

The talin2/β1D structure exhibits a well-defined N-terminal β tail helix extending from K752 to A773 (corresponding to K716-A737 in β3). This helix overlaps with a recent NMR structure of the β3 TM domain that exhibits a membrane-embedded helix extending to I721 and tilted by about 25° to the membrane bilayer (Lau *et al*, 2008b). Thus, β1D residues K752-I757 can be overlaid and merged with the membrane-

 

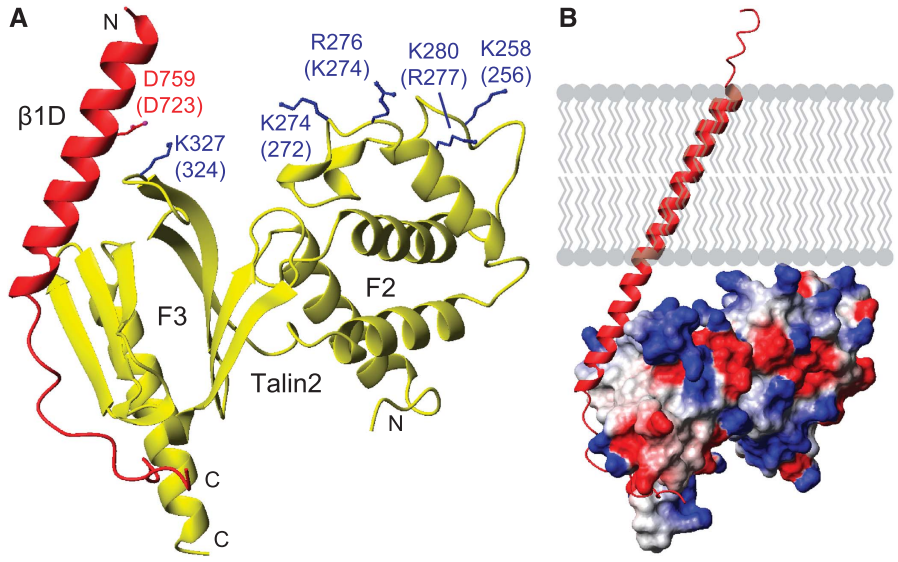


**Figure 2** The talin2/β1D structure. (**A**) One heterodimer from the crystal structure of talin2 F2–F3 bound to the β1D integrin tail. Labelling is for talin2/β1D with talin1/β3 numbering in parentheses. Highlighted residues interact with the membrane or form a key integrin/talin salt bridge. All structure images were generated with MOLMOL (Koradi *et al*, 1996). (**B**) The talin2/β1D structure was merged with the β3 transmembrane segment (PDB 2RMZ) (Lau *et al*, 2008b) and aligned to the calculated membrane tilt angle of 25°. The electrostatic potential is mapped on talin, illustrating the juxtaposition of several positively charged residues next to the membrane surface.

**Table II** Data collection and refinement statistics

| | |
|---|---|
| *Data collection* | |
| Beam line | ESRF ID23.EH2 |
| Space group | $P2_12_12_1$ |
| Cell parameters | $a = 53.26$ Å, $b = 108.72$ Å, $c = 131.85$ Å $\alpha = \beta = \gamma = 90^\circ$ |
| Wavelength (Å) | 0.8726 |
| Resolution (Å) | 41.95–2.17 (2.28–2.17)[a] |
| Total reflections | 154 133 (21 979) |
| Unique reflections | 41 362 (5982) |
| $R_{merge}$ | 0.114 (0.338) |
| Completeness (%) | 99.6 (99.9) |
| Multiplicity | 3.7 (3.7) |
| $I/\sigma(I)$ | 8.3 (3.5) |
| *Refinement* | |
| $R_{work}$ (%) | 21.3 |
| $R_{free}$ (%) | 24.9 |
| Overall mean $B$ values (Å$^2$) | 32.3 |
| Number of amino acid residues per asymmetric unit | 500 |
| Number of water molecules | 382 |
| Matthews coefficient | 3.05 (water content, 59.7%) |
| *RMSD from ideal values* | |
| Bonds/angles (Å/deg) | 0.005/0.874 |
| *Estimated error based on maximum likelihood* | |
| Coordinate/phase (Å/deg) | 0.32/25.1 |

[a]Highest resolution shell is shown in parenthesis.

embedded residues K716-I721 of the β3 TM structure, a procedure that could not be performed with the β3/PIPK1γ structure because of fraying of the integrin N-terminus in solution. The predicted orientation of the talin2/β1D structure with respect to the membrane (Figure 2B) results in the striking juxtaposition of a positively charged patch in the F2 domain (residues K258, K274, R276, and K280 in talin2; K256, K272, K274, and R277 in talin1) with the membrane (Figure 2A). These residues are conserved across species (Supplementary Figure S4), and we thus hypothesized that the residues forming this membrane orientation patch (MOP) have a key role in integrin activation.

This hypothesis was tested using a well-established αIIbβ3 integrin activation assay in CHO cells (Han *et al*, 2006) (Supplementary Figure S5). Expression of wild-type (wt) talin1 F3 slightly increased integrin activation, but expression of a longer talin1 construct with additional N-terminal domains (F1–F2–F3) caused a much more pronounced increase in integrin activation (Figure 3B). This activation was partially or fully abrogated by mutating the four MOP residues singly, doubly, or quadruply (4E) to glutamate (Figure 3A). To ensure that the observed effects were not because of protein instability, decreased integrin binding, or major structural changes, NMR studies were conducted on the 4E mutant. The mutations did not significantly affect integrin binding or the NMR spectrum of talin1 F2–F3, indicating that the 4E construct was folded and stable (Supplementary Figure S6). To test the generalizability of these findings, these experiments were repeated in CHO cells expressing a chimaeric integrin consisting of the extracellular and TM domains of αIIbβ3 and the intracellular domains of α5β1A (O'Toole *et al*, 1994) (Figure 3C). Consistent with previous findings (O'Toole *et al*, 1994; Bouaouina *et al*, 2008; Hato *et al*, 2008), the effect of talin on this integrin was reduced in comparison to αIIbβ3, owing to both higher basal activation and decreased maximal activation in response to talin. However, talin1 F1–F2–F3 did increase activation of this integrin, and this increase was abrogated by mutating MOP residues.

To show a direct interaction between the talin MOP and the membrane, we performed vesicle cosedimentation assays (Figure 4). A solution containing protein and vesicles was separated by centrifugation into a pellet consisting of the vesicles plus bound protein and a supernatant containing unbound material. In the presence of neutral phosphatidylcholine vesicles, talin1 F2–F3 remained in the unbound supernatant fraction. However, addition of 20% negatively

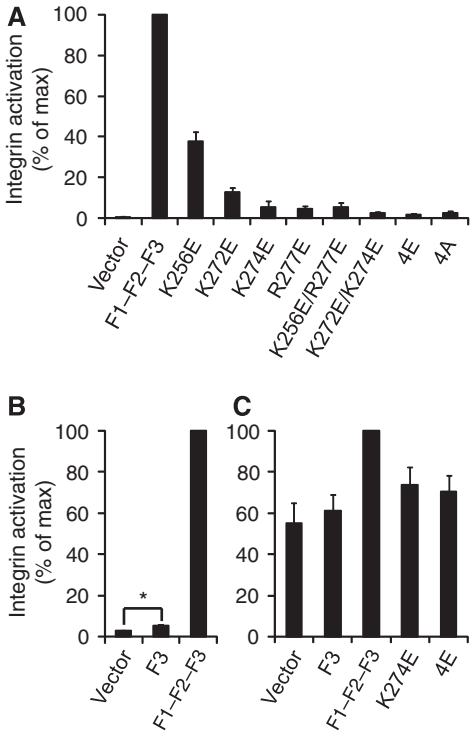


**Figure 3** A key role for a talin/membrane interaction in integrin activation. (**A**) GFP-talin1 F1–F2–F3 wild type (F1–F2–F3) or F1–F2–F3 with various mutations in the F2 domain were transfected into αIIbβ3-expressing CHO cells. Activated integrins were detected with PAC1 antibody and analysed by FACS 24 h after transfection. Integrin activity was normalized against GFP-F1–F2–F3 wt-transfected cells. Error bars represent standard errors of three independent experiments. 4E corresponds to all four membrane orientation patch (MOP) residues mutated to glutamate, and 4A corresponds to all four mutated to alanine. (**B**) As in (A), but with GFP-talin1 F3 wt or F1–F2–F3 wt. Error bars (barely visible because of small size) represent standard errors of two independent experiments. F3 caused a statistically significant increase in integrin activation (*) of $P = 0.0388$ by one tail test. (**C**) As in (A) and (B), but GFP-talin1 F3 wt, F1–F2-F3 wt, or F1–F2–F3 mutants were transfected into CHO cells expressing a chimaeric integrin containing the intracellular domains of α5β1A, as described in the text. Error bars represent standard errors of four independent experiments.

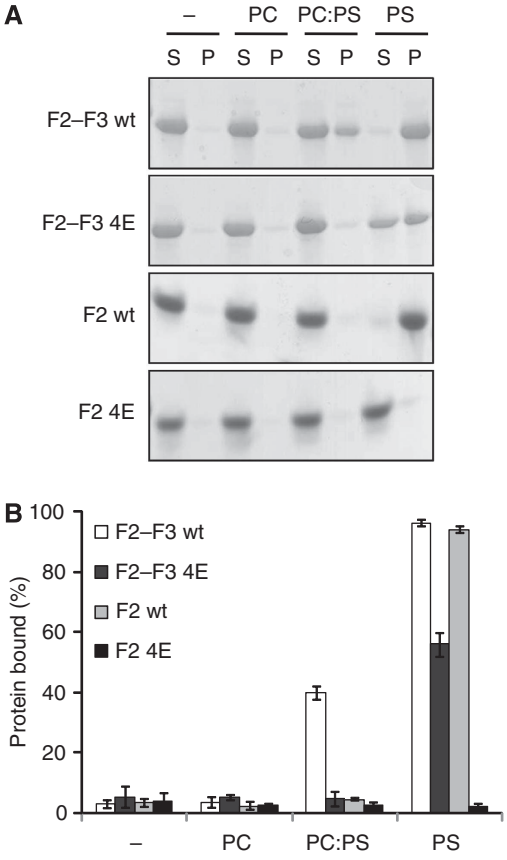


**Figure 4** The talin F2 domain membrane orientation patch (MOP) interacts with negatively charged membrane phospholipids. Talin1 F2–F3 and F2 (0.15 mg/ml), either wt or 4E, were mixed with vesicles (0.5 mg/ml) consisting of phosphatidylcholine (PC), phosphatidylserine (PS), or a 4:1 ratio of PC:PS and then centrifuged. (**A**) Coomassie-stained gel of one representative experiment. Unbound protein was located in the supernatant (S) and bound protein in the pellet (P). (**B**) Graphical representation of the percentage of protein bound to lipid vesicles (average of three independent experiments ± standard error).

charged phosphatidylserine to these vesicles caused 40% of talin1 F2–F3 to precipitate with the vesicles, and this binding was fully abrogated by the 4E mutation. Increasing the negatively charged content of the vesicles to 100% phosphatidylserine caused wt talin1 F2–F3 to be fully bound; the 4E mutation significantly decreased this binding, although some residual binding was still detected. Similar results were achieved with the talin1 F2 domain, although binding was only detected in 100% phosphatidylserine vesicles, and the 4E mutation fully abrogated vesicle binding. Thus, we have identified a specific new talin/membrane interaction site that is essential for full integrin activation and is sensitive to the presence of negatively charged moieties in the membrane.

### *The talin F3 domain forms a key membrane–proximal salt bridge with the β integrin tail*

The β1D/talin2 structure reveals a salt bridge between β1D D759 and talin2 K327 that caps the membrane–proximal portion of the interaction (Figure 2A). The distance between the aspartate side chain carboxyl oxygen atom and lysine side chain nitrogen atom is 3.7 Å (Supplementary Figure S3C). We note that this is a relatively large distance, but it is within the commonly used 4.0 Å limit (Barlow and Thornton, 1983; Kumar and Nussinov, 1999). This geometry is consistent between the two dimers in the asymmetric unit, and the electron density of these side chains is well defined (*B* values ranging from an average of 23 $Å^2$ for both $C_\beta$ atoms, to an average of 31 $Å^2$ for the aspartate side chain carboxyl oxygen atoms, and 45 $Å^2$ for the lysine nitrogen atom). An analysis of the β1D/talin2 by PISA (Krissinel and Henrick, 2007) predicts that β1D D759 and talin2 K327 contribute favourably to the overall interaction (data not shown).

These two residues are conserved in other paralogues of talin and integrins (Figure 1, D723 in β3 and K324 in talin1). NMR experiments show that swapping the charge of these residues in the β3/talin1 pair (D/R in β3 and K/D in talin1) abrogates the membrane–proximal interaction (Figure 5A–C) and decreases the affinity of the overall interaction (Supplementary Table II). A more conservative D/A mutation in β3 yields the same result, indicating that this is primarily

 

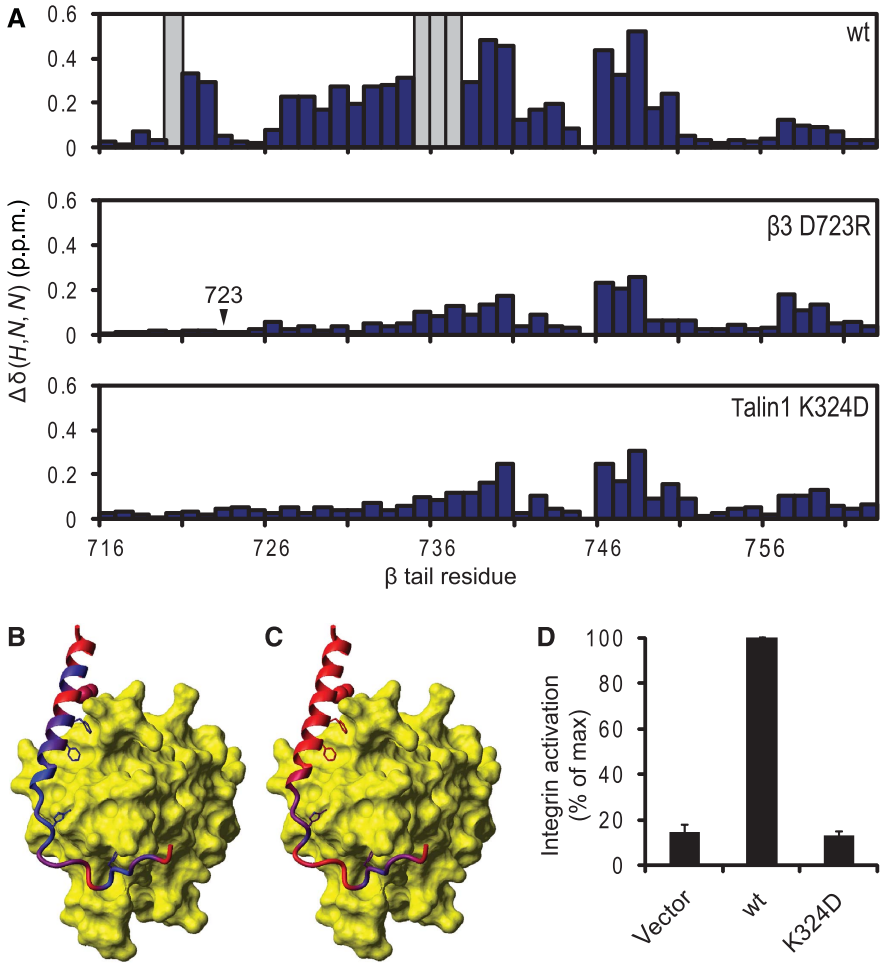


**Figure 5** A key salt bridge between talin and the β integrin tail. (**A**) Weighted shift maps of perturbations observed in $^{1}H$–$^{15}N$ HSQC spectra of the β3 tail on the addition of talin1 F3. Experiments were performed on β3 wt with talin1 wt, β3 D723R with talin1 wt, and β3 wt with talin1 K324D. Grey bars correspond to residues that could not be tracked because of exchange broadening. (**B**) Chemical shift perturbations in β3 on binding to talin1 F3 wt domain mapped onto the β1D/talin2 structure (largest shifts in blue, smallest in red). (**C**) As in (B) but with β3 D723R. (**D**) As in Figure 3A, but exploring the effect of talin1 F0–F1–F2–F3 wt or K324D on activation of αIIbβ3 expressed in CHO cells.

an electrostatic interaction (Supplementary Figure 7A). The effect of these mutations is virtually identical to that of a FF727/730AA mutation in the β3 membrane–proximal helix, which also abrogates integrin activation (Wegener *et al*, 2007) (Supplementary Figure S7A). A similar effect was observed with the β1A/talin1 pair (Supplementary Figures S7B and S8).

This same β3 residue, D723, has been shown earlier, by integrin activation assays (Hughes *et al*, 1996), α/β TM association studies (Kim *et al*, 2009), and NMR (Lau *et al*, 2009), to stabilize the integrin inactive state by interacting with R995 in αIIb. Talin1 K324 would thus compete with αIIb R995 for an electrostatic interaction with β3 D723, thereby weakening any αIIb R995–β3 D723 interaction (Figure 6A). This hypothesis was tested in αIIbβ3-expressing CHO cells. The addition of wt talin1 F0–F1–F2–F3 markedly increased integrin activation, but this increase was fully abrogated when talin1 K324D was introduced instead (Figure 5D). β3 D723 thus constrains bidirectional integrin signalling through an interaction with αIIb R995 in the absence of talin, but also participates in the activation process through an interaction with talin1 K324.

## Discussion

By exploring a wide range of talin/integrin interactions, we identified a talin/integrin pair (talin2/β1D) that binds much more tightly than any previously studied pair and was more amenable to crystallization. The resulting crystal structure hinted at novel interactions between the talin F2 domain and the cell membrane and between the talin F3 domain and a membrane–proximal aspartate residue in the β tail. We subsequently validated these interactions by additional biophysical methods and showed their biological relevance through in-cell experiments. These findings can now be incorporated into a new structural model of integrin activation by talin.

A recent NMR structure revealed that the αIIbβ3 integrin TM domains form a dimer of unique structure stabilized by two interactions: an outer membrane embrace that involves glycine-mediated packing of the two TM helices, and an inner membrane interface that includes the D723/R995 salt bridge and a conserved GFF motif in the α subunit (Lau *et al*, 2009). A structure generated by disulfide-based distance restraints and molecular modelling revealed a similar arrangement

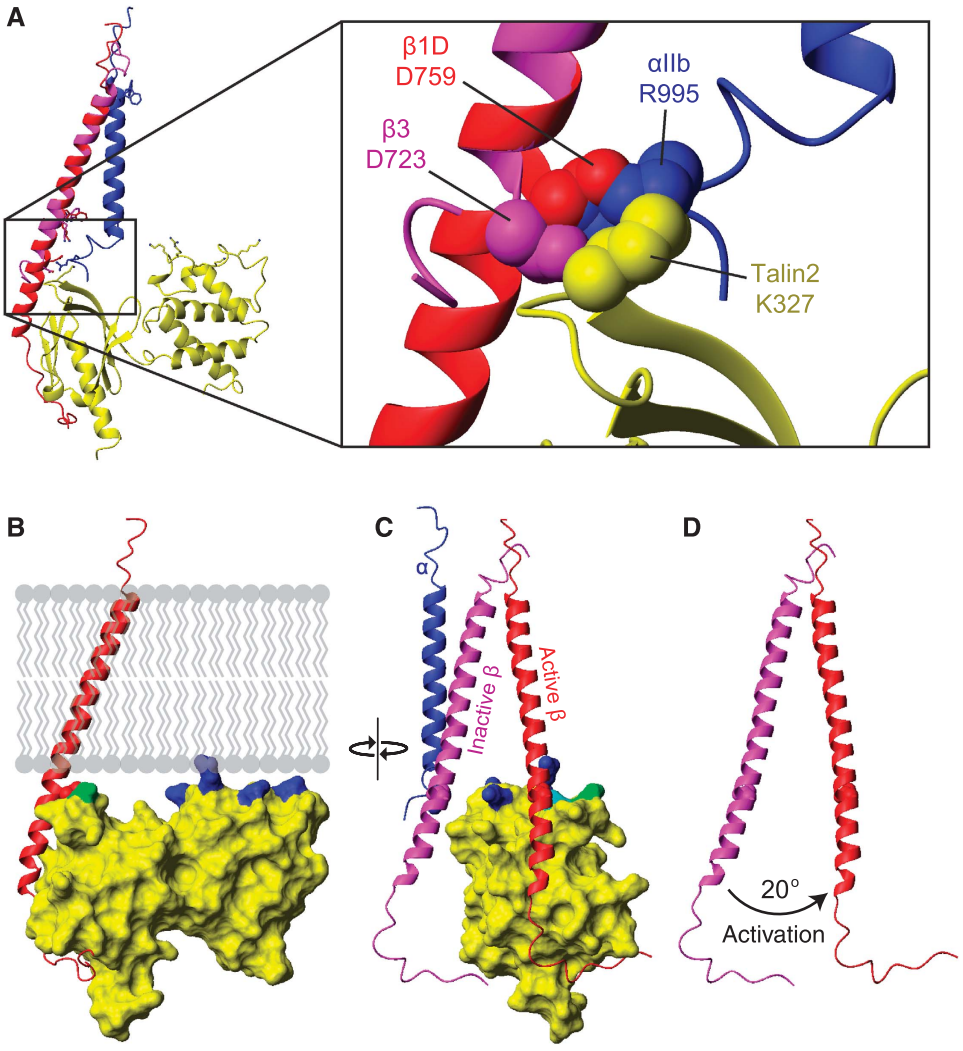


**Figure 6** Disruption of the α/β integrin dimer by talin. (**A**) Overlay of the talin2/β1D structure (plus β3 TM) with the αIIbβ3 TM structure (PDB 2K9J) (Lau *et al*, 2009). Talin is shown in yellow, αIIb in blue, β3/β1D bound to talin in red, and β3/β1D bound to αIIb in magenta. Inset shows inner membrane clasp competition. (**B**) The talin2/β1D structure (plus β3 TM) has been reoriented by 20° so that maximal contact is achieved between the membrane and the talin F2 membrane orientation patch (MOP). Membrane-targeting residues in F2 are highlighted in blue, and talin2 K325 (talin1 K322) in the F3 domain is highlighted in green. (**C**) The structure in (B) shown in an orthogonal 'back' view. The inactive αIIbβ3 transmembrane domain complex has been added to illustrate the change in β tilt angle on activation. The β3 TM structure has been extended into the cytoplasm by combining it with the β1D tail structure. Talin2 K327 (talin1 K324) is highlighted in cyan. (**D**) The same view as (C), but with only the two β integrin tails shown to highlight the 20° change in tilt angle.

(Zhu *et al*, 2009). An overlay of the talin2/β1D structure with the αIIbβ3 NMR structure reveals steric clashes between αIIb and talin2 located around the integrin inner membrane clasp (Figure 6A). Thus, the replacement of the interaction between β3 D723 (or β1 D759) and the α subunit with a β3 D723/talin interaction seems to be a key event in integrin activation. In addition, analysis of the talin2/β1D structure and mutation of the MOP residues showed the importance of this positively charge patch on F2. Closer inspection reveals that contact between the phospholipid headgroups of the membrane and the talin F2 MOP is better achieved if the tilt of the β TM domain changes by about 20° in a plane perpendicular to the plane of the membrane and to that of the initial β tilt (Figure 6B–D). The α subunit would be expected to remain in a vertical orientation, as it is constrained by tryptophan residues at each membrane interface (Yau *et al*, 1998; Lau *et al*, 2008a). An induced change in the β TM orientation would, however, disrupt the precise packing of the β subunit against the α TM domain. This 20° reorientation also brings K325 in the talin2 F3 domain (K322 in talin1) adjacent to the membrane, implying that the F2 MOP is a component of a larger membrane-interacting-charged surface, spanning multiple domains of talin. This is consistent with a previous report showing that mutation of this residue in talin1 disrupts integrin activation (Wegener *et al*, 2007); it could also explain why talin1 F2–F3 4E exhibits residual binding to membrane lipids (Figure 4).

Our results are therefore consistent with a model of integrin activation in which membrane-based reorientation, together with the weakened electrostatic interaction at the α/β cytoplasmic face, results in tail separation (Figure 7; Supplementary Movies S1 and S2). Indeed, this model explains why disruption of the αIIb R995–β3 D723 interaction is insufficient to activate integrins in the absence of talin binding (Tadokoro *et al*, 2003; Wegener *et al*, 2007) and is compatible with the observation that mutation of αIIb R995

 

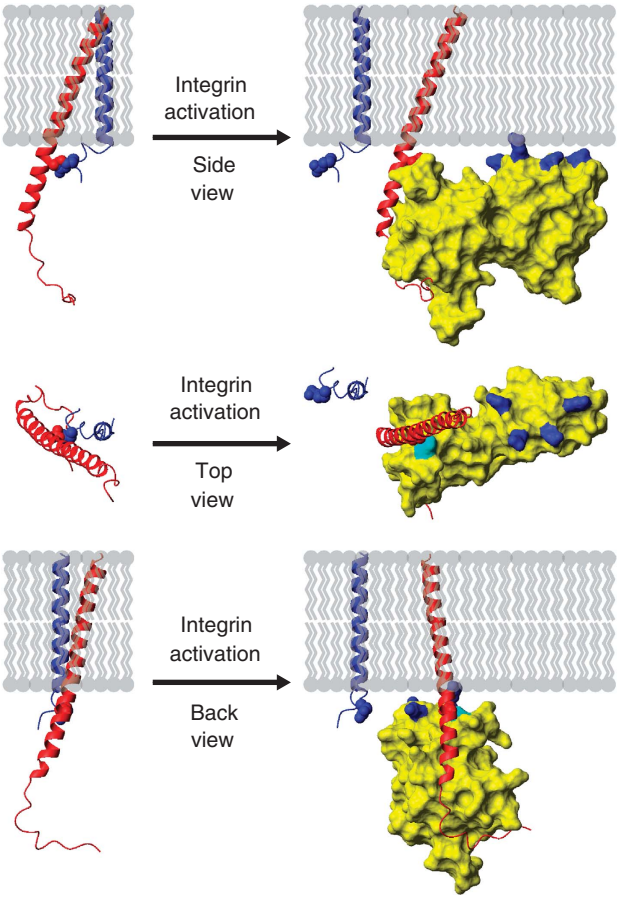


**Figure 7** Model of integrin activation by talin, shown in three orientations. When talin binds to the β integrin tail it forms an extensive interface with the tail, including a membrane–proximal salt bridge, disrupting the salt bridge between the α and β subunits. To maximize contacts between the membrane and the positively charged membrane orientation patch (MOP) on the talin F2 domain, the β integrin must be reoriented with respect to the membrane by approximately 20°. Through these actions talin causes α/β separation, inducing the active state in the extracellular region.

or β3 D723 weakens, but does not eliminate, α/β TM association (Kim *et al*, 2009; Lau *et al*, 2009). The α/β TM domains interact only weakly (Kim *et al*, 2009; Lau *et al*, 2009), and the ability of talin to induce α/β TM separation was recently shown directly (Kim *et al*, 2009), thus adding plausibility to the mechanism of activation reported here.

The fact that the relevant talin and integrin residues are highly conserved implies that this mechanism of integrin activation is generalizable across different isoforms. The sequences of the membrane–proximal regions of the β1 and β3 tails are remarkably similar (Figure 1A), and previous studies have showed that the D759A mutant in β1 increases integrin affinity for fibronectin (Sakai *et al*, 1998; Millon-Fremillon *et al*, 2008). Interestingly, mice with this knockin mutation in β1 do not display a pronounced phenotype (Czuchra *et al*, 2006). This could relate to the observation that though β3 integrins have more distinct 'on' and 'off' states, the activation of β1 integrins is more dynamically regulated, and β1 integrins exist in a more default 'on' state (Hynes, 2002; Hato *et al*, 2008). Thus, the combined effects of decreasing both α/β association and β/talin association by mutating D759 could compensate for one another in the case of β1 integrins. In contrast, the result of mutating D723 in β3 would be dominated by the effect of breaking its interaction with the α subunit. Even in β3 integrins, though, the effect of decreased talin interaction may partially counteract the effect of weakened α/β association, as αIIb R995D has a greater activating effect than β3 D723R (Hughes *et al*, 1996). Regardless, experiments with a chimaeric integrin containing the α5β1A cytoplasmic domains did reveal an essential role for the talin MOP in β1 integrin activation (Figure 3C). Compared with activation of αIIbβ3, talin caused a smaller increase in activation of the chimaeric α5β1A integrin—consistent with experiments reported on native α5β1A (Bouaouina *et al*, 2008)—but the effect of mutating MOP residues was the same as in αIIbβ3, largely abrogating talin-induced integrin activation.

In summary, this high-resolution structure of talin in complex with a full-length authentic integrin β cytoplasmic domain reveals that separation of the heterodimeric membrane-spanning helices is caused by the combined effects of talin-induced destabilization of the α/β inner membrane clasp and reorientation of the β TM domain. This model illustrates how localized membrane-specific protein interactions within the cell can lead to disruption of an interaction between TM helices in a large membrane-spanning receptor, effecting structural changes of great biological significance outside of the cell.

## Materials and methods

### *Preparation and purification of proteins*

Full-length β integrin tails were prepared as reported earlier for the β3 tail (Oxley *et al*, 2008). Specifically, using the In-Fusion cloning system (Clontech), β3 K716-T762, β1A K752-K798, and β1D K752-L801 were cloned into pET16b vectors modified with a 3C protease cleavage site between the N-terminal polyhistidine tag and the protein sequence. An additional construct of β1D K752-L801 was cloned into pET30b to produce the β1D integrin tail with a C-terminal polyhistidine tag (β1D-$His_6$). $^{15}$N-labelled β integrin tails were expressed into inclusion bodies in *Escherichia coli* grown in M9 minimal media containing $^{15}NH_4Cl$. Integrin tails were purified under denaturing conditions (50 mM sodium phosphate, 300 mM NaCl, 8 M urea, 0.035% β-mercaptoethanol, pH 7.0) by Talon immobilized metal affinity chromatography (Clontech), eluting the polyhistidine-tagged integrin tail in 200 mM imidazole. Further purification was performed by $C_4$ reverse phase HPLC. For constructs produced in pET16b, the polyhistidine tag was removed by cleavage with 3C protease, and the integrin tails were further purified by HPLC. Mutations in the β integrin tails and other constructs were introduced using the QuikChange kit (Stratagene).

The talin1 F2 (K196-G309), talin1 F3 (G309-S405), and talin2 F3 (G311-S408) domains were expressed using the pGEX-6P-2 vector in a manner similar to that reported earlier (de Pereda *et al*, 2005). In this case, *E. coli* was grown in Luria broth (LB) and was lysed in 50 mM Tris, 200 mM NaCl, 0.035% 2-mercaptoethanol, 0.4% Triton-X, pH 7.0. After glutathione sepharose chromatography and 3C cleavage, the protein was further purified by gel filtration chromatography into pH 7.0 NMR buffer (50 mM sodium phosphate, 100 mM NaCl, 1 mM DTT). The talin1 F2–F3 domains (K196-S405) and talin2 F2–F3 domains (K198-S408) were cloned into pET151 using traditional methods. They were expressed in *E. coli* grown in LB and lysed as for the F3 domain constructs, although in a different buffer (50 mM sodium phosphate, 300 mM NaCl, 0.035% β-mercaptoethanol, pH 7.0). Fusion proteins were purified with Talon resin, polyhistidine tags were removed by cleavage with TEV protease, and the proteins were further purified by gel filtration chromatography.

### *NMR spectroscopy*

All NMR experiments were performed on spectrometers equipped with Oxford Instruments superconducting magnets (500 and

600 MHz $^{1}$H operating frequencies) and GE/Omega computers. Unless otherwise indicated, samples were prepared in pH 6.1 NMR buffer with 5% $D_2O$ and Complete protease inhibitors (Roche). Experiments were performed at 25°C. The $^{1}$H and $^{15}$N resonances of $^{15}$N-labelled β integrin tails were assigned using a 1 mM sample in 20 mM sodium acetate pH 5.0 and using 3D NOESY-HSQC and 3D TOCSY-HSQC spectra. Resonance assignments were then transferred to pH 6.1 through pH titrations. Spectra were referenced in the direct dimension to DSS at 0 p.p.m., with indirect referencing in the $^{15}$N dimension using an $^{15}$N/$^{1}$H frequency ratio of 0.101329118 (Wishart *et al*, 1995). Data were processed using NMRPipe (Delaglio *et al*, 1995) and spectra were visualized using the program SPARKY (www.cgl.ucsf.edu/home/sparky) or CCPN Analysis (Vranken *et al*, 2005). Resonance assignments for β1D were first performed on β1D-His$_6$, because of higher expression levels, and assignments were transferred to untagged β1D.

$^{1}$H–$^{15}$N HSQC titrations were performed with 0.05 mM $^{15}$N-labelled integrin tail and increasing amounts of unlabelled talin, from 0 to 1 mM. Weighted combined $^{1}$H and $^{15}$N amide shifts ($\Delta(H,N)$) were calculated using the equation

$$\Delta(H, N) = \sqrt{\Delta_H W_H^2 + \Delta_N W_N^2},$$

where $W_H$ and $W_N$ are weighting factors for the $^{1}$H and $^{15}$N amide shifts, respectively ($W_H = 1$, $W_N = 0.154$) (Ayed *et al*, 2001) and $\Delta = \delta_{bound} - \delta_{free}$. Dissociation constants were determined by fitting changes in backbone chemical shift with concentration to the following equation:

$$\Delta(H, N) = \Delta(H, N)_{max} \frac{[L] + [U] + K_d - \sqrt{([L] + [U] + K_d)^2 - 4[L][U]}}{2[L]},$$

where $K_d$ is the dissociation constant, $\Delta(H,N)$ is the weighted shift change, $\Delta(H,N)_{max}$ is the shift change at saturation, and $[L]$ and $[U]$ are the concentrations of the labelled and unlabelled proteins, respectively. Data from peaks that were well resolved, had a significant change in position, and were discernable throughout the titration were fit simultaneously to this equation with the program OriginPro 8, extracting a single $K_d$ and multiple $\Delta(H,N)_{max}$ values.

### *Crystallization*

Samples for crystallization contained 6 mg/ml (250 μM) talin2 F2–F3 and 3 mg/ml (500 μM) β1D integrin tail in crystallization buffer (10 mM Tris, 100 mM NaCl, pH 7.0). Crystals were grown by the sitting drop method at 4°C in 0.1 M ammonium acetate, 0.02 M magnesium chloride, 0.05 M HEPES (pH 7.0), and 5% PEG 8k. For data collection, crystals were soaked in the same buffer plus 30% glycerol and then flash frozen in liquid nitrogen.

Data were collected at the ESRF on beamline ID23.EH2 at a wavelength of 0.8726 Å. The crystal diffracted to 2.17 Å resolution. Data were indexed and integrated using MOSFLM, and scaled and merged using SCALA from the CCP4 program suite (Collaborative Computational Project Number 4, 1994). The structure was phased by molecular replacement using the talin1 F2–F3 domains from PDB entries 1MIX, 1MK7, and 1MK9 (Garcia-Alvarez *et al*, 2003) as search models and using the program Phaser (Read, 2001). The crystal indexed to the space group $P2_12_12_1$ and contained two integrin/talin dimers in the asymmetric unit. Model building was performed in Coot (Emsley and Cowtan, 2004), and refinement in Refmac (Winn *et al*, 2003) and PHENIX Refine (Adams *et al*, 2002). Noncrystallographic symmetry restraints were included only in the initial stages of refinement. The integrin tail was not included in the original molecular replacement model, but it could be built into electron density early in the refinement process. The structure refined to $R_{work} = 21.30\%$ and $R_{free} = 24.85\%$. In a Ramachandran plot, 91.2% of residues lie in favoured regions, 8.6% in allowed regions, 0.2% in generously allowed regions, and 0.0% in disallowed regions.

### *Integrin activation assays*

PAC1 binding was measured by two-colour flow cytometry as described earlier (Han *et al*, 2006). In brief, A5 cells (CHO cells expressing integrin αIIbβ3) were transfected with N-terminal GFP fused talin1 F3 or F1–F2–F3 constructs, or co-transfected with GFP and Talin F0–F1–F2–F3 constructs. Experiments were similarly performed on CHO cells expressing a chimaeric integrin consisting of the extracellular and TM domains of αIIbβ3 and the intracellular domains of α5β1A, which has been described earlier (O'Toole *et al*, 1994). Twenty-four hours after talin transfection, cells were collected, incubated with activation-specific anti-αIIbβ3 antibody PAC1 (Shattil *et al*, 1985), and then stained by R-phycoerythrin-conjugated anti-IgM antibody. Five minutes before analysis, propidium iodide (PI) was added, and PAC1 binding was measured with FACSCalibur (BD Bioscience). Only GFP-positive and PI-negative cells (live cells) were analysed to calculate the level of integrin activation. The ability of talin constructs containing various mutations to activate integrins was presented as percent of maximal integrin activation, and was calculated as (Fo−Fr)/(Fmax−Fr), where Fo is the mean fluorescence intensity (MFI) of PAC1 binding of various mutant-transfected cells, Fr is the MFI of PAC1 binding in the presence of competitive inhibitor eptifibatide (Scarborough *et al*, 1993), and Fmax is the MFI of PAC1 binding of wt F1–F2–F3 or F0–F1–F2–F3-transfected cells.

### *Phospholipid cosedimentation assays*

Large multilamellar vesicles were prepared essentially as described earlier (Niggli *et al*, 1994). Briefly, films of dried phospholipids (Sigma) were swollen at 5 mg/ml in 20 mM Hepes (pH 7.4), 0.2 mM EGTA for 3 h at 42°C. The vesicles were then centrifuged (20 000 *g* for 20 min at 4°C), and the pellet was resuspended in the same buffer at 5 mg/ml. Protein samples were diluted into 20 mM Tris/HCl (pH 7.4), 0.1 mM EDTA, 15 mM β-mercaptoethanol. After centrifugation (20 000 *g* for 20 min at 4°C) proteins (0.15 mg/ml) were incubated (30 min, 25°C) in the absence or presence of phospholipid vesicles (0.5 mg/ml), 200 μl total volume, followed by centrifugation (25 000 *g* for 20 min at 4°C). Pellet and supernatant fractions were subjected to SDS–PAGE and proteins detected by Coomassie-blue staining. The percentage of protein bound (protein in pellet/total protein) was calculated by measuring band density in ImageJ (Abramoff *et al*, 1994).

### *Accession codes*

Atomic coordinates for the talin2/β1D complex have been deposited in the Protein Data Bank under accession number 3G9W. Chemical shift resonance assignments have been deposited in the Biological Magnetic Resonance Bank (BMRB) under the following accession numbers: 16159 (β1A), 16158 (β1D), and 16162 (β1D-His$_6$). Assignments for β3 have been reported earlier (Oxley *et al*, 2008) and deposited in the BMRB under accession number 15552.

### *Supplementary data*

Supplementary data are available at *The EMBO Journal* Online (http://www.embojournal.org).

## Acknowledgements

We thank Tobias Ulmer for providing the coordinates of the αIIbβ3 transmembrane structure. This work was supported by funding from the Wellcome Trust (IDC and DRC), the NIH (grants HL078784 and AR27214 to MHG), Cancer Research UK (DRC), the Rhodes Trust (NJA), the NIH Cell Migration Consortium (IDC, MHG, and KLW), the Marie Curie Fellowship program (IV), and Trinity College Oxford (IV).

## Conflict of interest

The authors declare that they have no conflict of interest.

## References

Abramoff MD, Magelhaes PJ, Ram SJ (1994) Image processing with ImageJ. *Biophoton Int* **11:** 36–42

Adams PD, Grosse-Kunstleve RW, Hung LW, Ioerger TR, McCoy AJ, Moriarty NW, Read RJ, Sacchettini JC, Sauter NK, Terwilliger TC

(2002) PHENIX: building new software for automated crystallographic structure determination. *Acta Crystallogr D Biol Crystallogr* **58**(Part 11)**:** 1948–1954

Arnaout MA, Goodman SL, Xiong JP (2007) Structure and mechanics of integrin-based cell adhesion. *Curr Opin Cell Biol* **19:** 495–507

Askari JA, Buckley PA, Mould AP, Humphries MJ (2009) Linking integrin conformation to function. *J Cell Sci* **122** (Part 2)**:** 165–170

Ayed A, Mulder FA, Yi GS, Lu Y, Kay LE, Arrowsmith CH (2001) Latent and active p53 are identical in conformation. *Nat Struct Biol* **8:** 756–760

Barlow DJ, Thornton JM (1983) Ion-pairs in proteins. *J Mol Biol* **168:** 867–885

Barsukov IL, Prescot A, Bate N, Patel B, Floyd DN, Bhanji N, Bagshaw CR, Letinic K, Di Paolo G, De Camilli P, Roberts GC, Critchley DR (2003) Phosphatidylinositol phosphate kinase type 1gamma and beta1-integrin cytoplasmic domain bind to the same region in the talin FERM domain. *J Biol Chem* **278:** 31202–31209

Belkin AM, Zhidkova NI, Balzac F, Altruda F, Tomatis D, Maier A, Tarone G, Koteliansky VE, Burridge K (1996) Beta 1D integrin displaces the beta 1A isoform in striated muscles: localization at junctional structures and signaling potential in nonmuscle cells. *J Cell Biol* **132:** 211–226

Bouaouina M, Lad Y, Calderwood DA (2008) The N-terminal domains of talin cooperate with the phosphotyrosine binding-like domain to activate beta1 and beta3 integrins. *J Biol Chem* **283:** 6118–6125

Calderwood DA (2004) Integrin activation. *J Cell Sci* **117** (Part 5)**:** 657–666

Calderwood DA, Fujioka Y, de Pereda JM, Garcia-Alvarez B, Nakamoto T, Margolis B, McGlade CJ, Liddington RC, Ginsberg MH (2003) Integrin beta cytoplasmic domain interactions with phosphotyrosine-binding domains: a structural prototype for diversity in integrin signaling. *Proc Natl Acad Sci USA* **100:** 2272–2277

Calderwood DA, Yan B, de Pereda JM, Alvarez BG, Fujioka Y, Liddington RC, Ginsberg MH (2002) The phosphotyrosine binding-like domain of talin activates integrins. *J Biol Chem* **277:** 21749–21758

Campbell ID, Ginsberg MH (2004) The talin-tail interaction places integrin activation on FERM ground. *Trends Biochem Sci* **29:** 429–435

Collaborative Computational Project Number 4 (1994) The CCP4 suite: programs for protein crystallography. *Acta Crystallogr D Biol Crystallogr* **50**(Part 5)**:** 760–763

Conti FJ, Felder A, Monkley S, Schwander M, Wood MR, Lieber R, Critchley D, Muller U (2008) Progressive myopathy and defects in the maintenance of myotendinous junctions in mice that lack talin 1 in skeletal muscle. *Development* **135:** 2043–2053

Critchley DR, Gingras AR (2008) Talin at a glance. *J Cell Sci* **121** (Part 9)**:** 1345–1347

Czuchra A, Meyer H, Legate KR, Brakebusch C, Fassler R (2006) Genetic analysis of beta1 integrin 'activation motifs' in mice. *J Cell Biol* **174:** 889–899

de Pereda JM, Wegener KL, Santelli E, Bate N, Ginsberg MH, Critchley DR, Campbell ID, Liddington RC (2005) Structural basis for phosphatidylinositol phosphate kinase type Igamma binding to talin at focal adhesions. *J Biol Chem* **280:** 8381–8386

Delaglio F, Grzesiek S, Vuister GW, Zhu G, Pfeifer J, Bax A (1995) NMRPipe: a multidimensional spectral processing system based on UNIX pipes. *J Biomol NMR* **6:** 277–293

Emsley P, Cowtan K (2004) Coot: model-building tools for molecular graphics. *Acta Crystallogr D Biol Crystallogr* **60**(Part 12 Part 1)**:** 2126–2132

Garcia-Alvarez B, de Pereda JM, Calderwood DA, Ulmer TS, Critchley D, Campbell ID, Ginsberg MH, Liddington RC (2003) Structural determinants of integrin recognition by talin. *Mol Cell* **11:** 49–58

Ginsberg MH, Partridge A, Shattil SJ (2005) Integrin regulation. *Curr Opin Cell Biol* **17:** 509–516

Han J, Lim CJ, Watanabe N, Soriani A, Ratnikov B, Calderwood DA, Puzon-McLaughlin W, Lafuente EM, Boussiotis VA, Shattil SJ, Ginsberg MH (2006) Reconstructing and deconstructing agonist-induced activation of integrin alphaIIbbeta3. *Curr Biol* **16:** 1796–1806

Hato T, Yamanouchi J, Tamura T, Yakushijin Y, Sakai I, Yasukawa M (2008) Cooperative role of the membrane-proximal and -distal residues of the integrin beta3 cytoplasmic domain in regulation of talin-mediated alpha IIb beta3 activation. *J Biol Chem* **283:** 5662–5668

Hughes PE, Diaz-Gonzalez F, Leong L, Wu C, McDonald JA, Shattil SJ, Ginsberg MH (1996) Breaking the integrin hinge. A defined structural constraint regulates integrin signaling. *J Biol Chem* **271:** 6571–6574

Hughes PE, O'Toole TE, Ylanne J, Shattil SJ, Ginsberg MH (1995) The conserved membrane-proximal region of an integrin cytoplasmic domain specifies ligand binding affinity. *J Biol Chem* **270:** 12411–12417

Hynes RO (2002) Integrins: bidirectional, allosteric signaling machines. *Cell* **110:** 673–687

Kim C, Lau TL, Ulmer TS, Ginsberg MH (2009) Interactions of platelet integrin alphaIIb and beta3 transmembrane domains in mammalian cell membranes and their role in integrin activation. *Blood* **113:** 4747–4753

Kim M, Carman CV, Springer TA (2003) Bidirectional transmembrane signaling by cytoplasmic domain separation in integrins. *Science* **301:** 1720–1725

Koradi R, Billeter M, Wuthrich K (1996) MOLMOL: a program for display and analysis of macromolecular structures. *J Mol Graph* **14:** 51–55, 29–32

Krissinel E, Henrick K (2007) Inference of macromolecular assemblies from crystalline state. *J Mol Biol* **372:** 774–797

Kumar S, Nussinov R (1999) Salt bridge stability in monomeric proteins. *J Mol Biol* **293:** 1241–1255

Lau TL, Dua V, Ulmer TS (2008a) Structure of the integrin alphaIIb transmembrane segment. *J Biol Chem* **283:** 16162–16168

Lau TL, Kim C, Ginsberg MH, Ulmer TS (2009) The structure of the integrin alphaIIbbeta3 transmembrane complex explains integrin transmembrane signalling. *EMBO J* **28:** 1351–1361

Lau TL, Partridge AW, Ginsberg MH, Ulmer TS (2008b) Structure of the integrin beta3 transmembrane segment in phospholipid bicelles and detergent micelles. *Biochemistry* **47:** 4008–4016

Lu C, Takagi J, Springer TA (2001) Association of the membrane proximal regions of the alpha and beta subunit cytoplasmic domains constrains an integrin in the inactive state. *J Biol Chem* **276:** 14642–14648

Luo BH, Carman CV, Springer TA (2007) Structural basis of integrin regulation and signaling. *Annu Rev Immunol* **25:** 619–647

Millon-Fremillon A, Bouvard D, Grichine A, Manet-Dupe S, Block MR, Albiges-Rizo C (2008) Cell adaptive response to extracellular matrix density is controlled by ICAP-1-dependent beta1-integrin affinity. *J Cell Biol* **180:** 427–441

Nieswandt B, Moser M, Pleines I, Varga-Szabo D, Monkley S, Critchley D, Fassler R (2007) Loss of talin1 in platelets abrogates integrin activation, platelet aggregation, and thrombus formation *in vitro* and *in vivo*. *J Exp Med* **204:** 3113–3118

Niggli V, Kaufmann S, Goldmann WH, Weber T, Isenberg G (1994) Identification of functional domains in the cytoskeletal protein talin. *Eur J Biochem* **224:** 951–957

O'Toole TE, Katagiri Y, Faull RJ, Peter K, Tamura R, Quaranta V, Loftus JC, Shattil SJ, Ginsberg MH (1994) Integrin cytoplasmic domains mediate inside-out signal transduction. *J Cell Biol* **124:** 1047–1059

Oxley CL, Anthis NJ, Lowe ED, Vakonakis I, Campbell ID, Wegener KL (2008) An integrin phosphorylation switch: the effect of beta3 integrin tail phosphorylation on Dok1 and talin binding. *J Biol Chem* **283:** 5420–5426

Partridge AW, Liu S, Kim S, Bowie JU, Ginsberg MH (2005) Transmembrane domain helix packing stabilizes integrin alphaIIbbeta3 in the low affinity state. *J Biol Chem* **280:** 7294–7300

Petrich BG, Fogelstrand P, Partridge AW, Yousefi N, Ablooglu AJ, Shattil SJ, Ginsberg MH (2007a) The antithrombotic potential of selective blockade of talin-dependent integrin alpha IIb beta 3 (platelet GPIIb-IIIa) activation. *J Clin Invest* **117:** 2250–2259

Petrich BG, Marchese P, Ruggeri ZM, Spiess S, Weichert RA, Ye F, Tiedt R, Skoda RC, Monkley SJ, Critchley DR, Ginsberg MH (2007b) Talin is required for integrin-mediated platelet function in hemostasis and thrombosis. *J Exp Med* **204:** 3103–3111

Read RJ (2001) Pushing the boundaries of molecular replacement with maximum likelihood. *Acta Crystallogr D Biol Crystallogr* **57**(Part 10)**:** 1373–1382

Sakai T, Zhang Q, Fassler R, Mosher DF (1998) Modulation of beta1A integrin functions by tyrosine residues in the beta1 cytoplasmic domain. *J Cell Biol* **141:** 527–538

Scarborough RM, Naughton MA, Teng W, Rose JW, Phillips DR, Nannizzi L, Arfsten A, Campbell AM, Charo IF (1993) Design of potent and specific integrin antagonists. Peptide antagonists with high specificity for glycoprotein IIb-IIIa. *J Biol Chem* **268:** 1066–1073

Senetar MA, Moncman CL, McCann RO (2007) Talin2 is induced during striated muscle differentiation and is targeted to stable adhesion complexes in mature muscle. *Cell Motil Cytoskeleton* **64:** 157–173

Shattil SJ, Hoxie JA, Cunningham M, Brass LF (1985) Changes in the platelet membrane glycoprotein IIb.IIIa complex during platelet activation. *J Biol Chem* **260:** 11107–11114

Tadokoro S, Shattil SJ, Eto K, Tai V, Liddington RC, de Pereda JM, Ginsberg MH, Calderwood DA (2003) Talin binding to integrin beta tails: a final common step in integrin activation. *Science* **302:** 103–106

Takagi J, Erickson HP, Springer TA (2001) C-terminal opening mimics 'inside-out' activation of integrin alpha5beta1. *Nat Struct Biol* **8:** 412–416

Ulmer TS, Calderwood DA, Ginsberg MH, Campbell ID (2003) Domain-specific interactions of talin with the membrane-proximal region of the integrin beta3 subunit. *Biochemistry* **42:** 8307–8312

Vinogradova O, Velyvis A, Velyviene A, Hu B, Haas T, Plow E, Qin J (2002) A structural mechanism of integrin alpha(IIb)beta(3) 'inside-out' activation as regulated by its cytoplasmic face. *Cell* **110:** 587–597

Vranken WF, Boucher W, Stevens TJ, Fogh RH, Pajon A, Llinas M, Ulrich EL, Markley JL, Ionides J, Laue ED (2005) The CCPN data model for NMR spectroscopy: development of a software pipeline. *Proteins* **59:** 687–696

Wegener KL, Campbell ID (2008) Transmembrane and cytoplasmic domains in integrin activation and protein-protein interactions (review). *Mol Membr Biol* **25:** 376–387

Wegener KL, Partridge AW, Han J, Pickford AR, Liddington RC, Ginsberg MH, Campbell ID (2007) Structural basis of integrin activation by talin. *Cell* **128:** 171–182

Winn MD, Murshudov GN, Papiz MZ (2003) Macromolecular TLS refinement in REFMAC at moderate resolutions. *Methods Enzymol* **374:** 300–321

Wishart DS, Bigam CG, Yao J, Abildgaard F, Dyson HJ, Oldfield E, Markley JL, Sykes BD (1995) 1H, 13C and 15N chemical shift referencing in biomolecular NMR. *J Biomol NMR* **6:** 135–140

Yau WM, Wimley WC, Gawrisch K, White SH (1998) The preference of tryptophan for membrane interfaces. *Biochemistry* **37:** 14713–14718

Zhu J, Luo BH, Barth P, Schonbrun J, Baker D, Springer TA (2009) The structure of a receptor with two associating transmembrane domains on the cell surface: integrin alphaIIbbeta3. *Mol Cell* **34:** 234–249

 

## Supplementary Data

**Supplementary Figure S1** Chemical shift perturbation experiments with integrin tails. (**A**) $^{1}H$-$^{15}N$ HSQC spectra of 0.05 mM $^{15}N$-labelled β3 tail with increasing concentrations of talin1 F3 domain: 0 mM (red), 0.025 mM (tomato), 0.05 mM (orange), 0.1 mM (yellow), 0.2 mM (green), 0.4 mM (cyan), 0.6 mM (blue), 0.8 mM (purple), 1 mM (magenta). (**B**) $^{1}H$-$^{15}N$ HSQC spectra of 0.05 mM $^{15}N$-labelled β1D tail with increasing concentrations of talin2 F3 domain: 0 mM (red), 0.0125 mM (tomato), 0.025 mM (orange), 0.05 mM (yellow), 0.075 mM (green), 0.1 mM (cyan), 0.2 mM (blue), 0.5 mM (purple), 1 mM (magenta). A few peaks broaden out due to intermediate exchange, but many of these can still be traced when the contour levels are taken lower. (**C**) Binding curves used for $K_d$ calculation. Peaks were tracked through HSQC spectra of $^{15}N$-labelled β tail acquired with increasing concentrations of talin F3 domain. For each trackable peak, the change in chemical shift was normalized to the change at 1 mM talin. Note that while $K_d$ values were determined by fitting several curves simultaneously, for clarity each value plotted here shows the average of several peaks ± standard error.

**Supplementary Figure S2** Comparisons of the talin2 and talin1 structures. (**A**) Asymmetric unit of the crystal structure of talin2 F2-F3 bound to the β1D integrin tail, shown in two orthogonal orientations. The integrin tail is shown in red, the talin2 F3 domain in yellow, and the talin2 F2 domain in cyan or magenta. (**B**) Structure of talin2 F2-F3 (yellow) aligned with the F2-F3 domains of talin1 from PDB 1MK9 (cyan) (Garcia-Alvarez et al, 2003). (**C**) Structure of β1D (red) bound to talin2 F2-F3 (yellow) aligned to the structure of the β3/PIPK1γ peptide (magenta) bound to talin1 F3 (cyan) from PDB 2H7E (Wegener et al, 2007). The alignment used the backbone of the talin1 F3 domain. It is shown in two orthogonal views, and key residues are highlighted.

**Supplementary Figure S3** Electron Density Maps From the β1D/Talin2 Crystal Structure. (**A**) The NPxY motif of β1D, showing distinct electron density (sigma 1.2). (**B**) A portion of the β1D membrane-proximal helix, showing distinct electron density (sigma 1.2). (**C**) The membrane-proximal salt bridge, showing distinct electron density (sigma 1.2). The side chain nitrogen of talin2 K327 and the side chain oxygen of β1D D759 are separated by 3.70 Å. Electron density map images were generated in Coot (Emsley & Cowtan, 2004).

**Supplementary Figure S4** Alignment of talin head domain sequences from different organisms. The amino acid sequence of talin isoforms from various organisms were aligned using ClustalW (Larkin et al, 2007). Only the sequence of the N-terminal head domain is shown. Residues located in the membrane orientation patch (MOP) in the F2 domain or involved in a key talin/integrin salt bridge are highlighted and labelled with vertebrate talin1 numbering. These residues are conserved in all talin sequences tested.

**Supplementary Figure S5** Representative integrin activation assay raw data. (**A**) A set of raw FACS data from one of the three independent experiments conducted for Figure 1c. Dot plots correlate integrin activation (PAC1 antibody signal) with GFP-talin F1-F2-F3 expression in CHO cells expressing αIIbβ3. This correlation is pronounced for talin wt, but mutations that disrupt the talin membrane orientation patch (MOP)

diminish this effect. See Materials and Methods for full experimental details. (**B**) Western blot showing expression levels of constructs tested.

**Supplementary Figure S6** Talin F2 mutants do not affect talin integrity or integrin binding. (**A**) 1D NMR spectra of 1 mM talin1 F2-F3 wt and the 4E mutant in which K256, K272, K274, and R277 in F2 were substituted with glutamates. Both spectra are indicative of a folded protein and do not display major differences. (**B**) Chemical shift perturbation maps for 0.05 mM β3 titrated with 1 mM talin1 F3 wt, F2-F3 wt, and F2-F3 4E. $K_d$ values for the interactions are shown. No major differences were observed between the different constructs.

**Supplementary Figure S7** Mutations that abrogate talin binding to the membrane-proximal region of the β integrin tail. (**A**) Chemical shift perturbation maps for $^{15}$N-labelled wt and mutant β3 tail (0.05 mM) titrated with 1 mM talin1 F3 domain. Mutants of β3 tested were D723R, D723A, and FF727/730AA. (**B**) As in panel A but with β1A wt, D723R and FF763/766AA.

**Supplementary Figure S8** Disrupting the membrane-proximal salt bridge between β1A and talin1. (**A**) Weighted shift maps of perturbations observed in $^{1}$H-$^{15}$N HSQC spectra of the β1A tail upon the addition of talin1 F3. Experiments were performed on β1A wt with talin1 wt, β1A D759R with talin1 wt, and β1A wt with talin1 K324D. Grey bars correspond to residues that could not be tracked due to exchange broadening. (**B**) Chemical shift perturbations in β1A upon binding to talin1 F3 wt domain mapped onto the β1D/talin2 structure (largest shifts in blue, smallest in red). (**C**) As in panel B but with β1A D723R.

**Supplementary Movie S1** A top view of integrin activation. This movie shows a proposed mechanism of integrin activation by talin, viewed looking down through the membrane. Talin binds to the β integrin tail and disrupts the α/β inner membrane clasp. It then tilts the integrin tail by about 20° to maximize contact between the positively charged membrane orientation patch on the F2 domain, further disrupting the α/β interaction and causing tail separation. Atoms in the α and β integrins located within 4 Å of an atom on the other integrin have been highlighted, allowing the breaking of α/β contacts to be visualized as integrin activation proceeds.

**Supplementary Movie S2** A side view of integrin activation. Same as Supplementary Movie S1, but viewed from the side, along the cell membrane.

**Supplementary Table I** Backbone RMSD values for alignment of talin2 with various talin1 structures

| Talin1 structure | F2-F3 (209-398) | F2 (209-304) | F3 (311-398) |
|---|---|---|---|
| 1MK9 | 1.002 | 0.520 | 1.125 |
| 1MK7 | 1.110 | 0.697 | 1.194 |
| 1MIX | 1.396 | 0.638 | 1.858 |
| 2H7E | - | - | 1.056 |

RMSD values are given in Å and were calculated with MOLMOL (Koradi et al, 1996).

**Supplementary Table II** $K_d$ values for the interaction of talin1 F3 with the β3 integrin tail For wild type proteins and salt bridge-breaking mutants

| | $K_d$ (μM)[a] | ΔΔG (kJ/mol)[b] |
|---|---|---|
| wt | 273 ± 6 | - |
| β3 D723R | 970 ± 26 | 3.1 |
| talin1 K324D | 800 ± 14 | 2.7 |

[a]$K_d$ values are given in μM, ± standard error.
[b]ΔG was calculated from $K_d$ for each interaction, and ΔΔG was calculated by subtracting ΔG of that interaction from ΔG of the interaction involving the wild type tail (a positive value denotes a decrease in affinity).

## Supplementary References

Emsley P, Cowtan K (2004) Coot: model-building tools for molecular graphics. *Acta Crystallogr D Biol Crystallogr* **60**(Pt 12 Pt 1)**:** 2126-2132

Garcia-Alvarez B, de Pereda JM, Calderwood DA, Ulmer TS, Critchley D, Campbell ID, Ginsberg MH, Liddington RC (2003) Structural determinants of integrin recognition by talin. *Mol Cell* **11**(1)**:** 49-58

Koradi R, Billeter M, Wuthrich K (1996) MOLMOL: a program for display and analysis of macromolecular structures. *J Mol Graph* **14**(1)**:** 51-55, 29-32

Larkin MA, Blackshields G, Brown NP, Chenna R, McGettigan PA, McWilliam H, Valentin F, Wallace IM, Wilm A, Lopez R, Thompson JD, Gibson TJ, Higgins DG (2007) Clustal W and Clustal X version 2.0. *Bioinformatics* **23**(21)**:** 2947-2948

Wegener KL, Partridge AW, Han J, Pickford AR, Liddington RC, Ginsberg MH, Campbell ID (2007) Structural basis of integrin activation by talin. *Cell* **128**(1)**:** 171-182

## Supplementary Figure S1

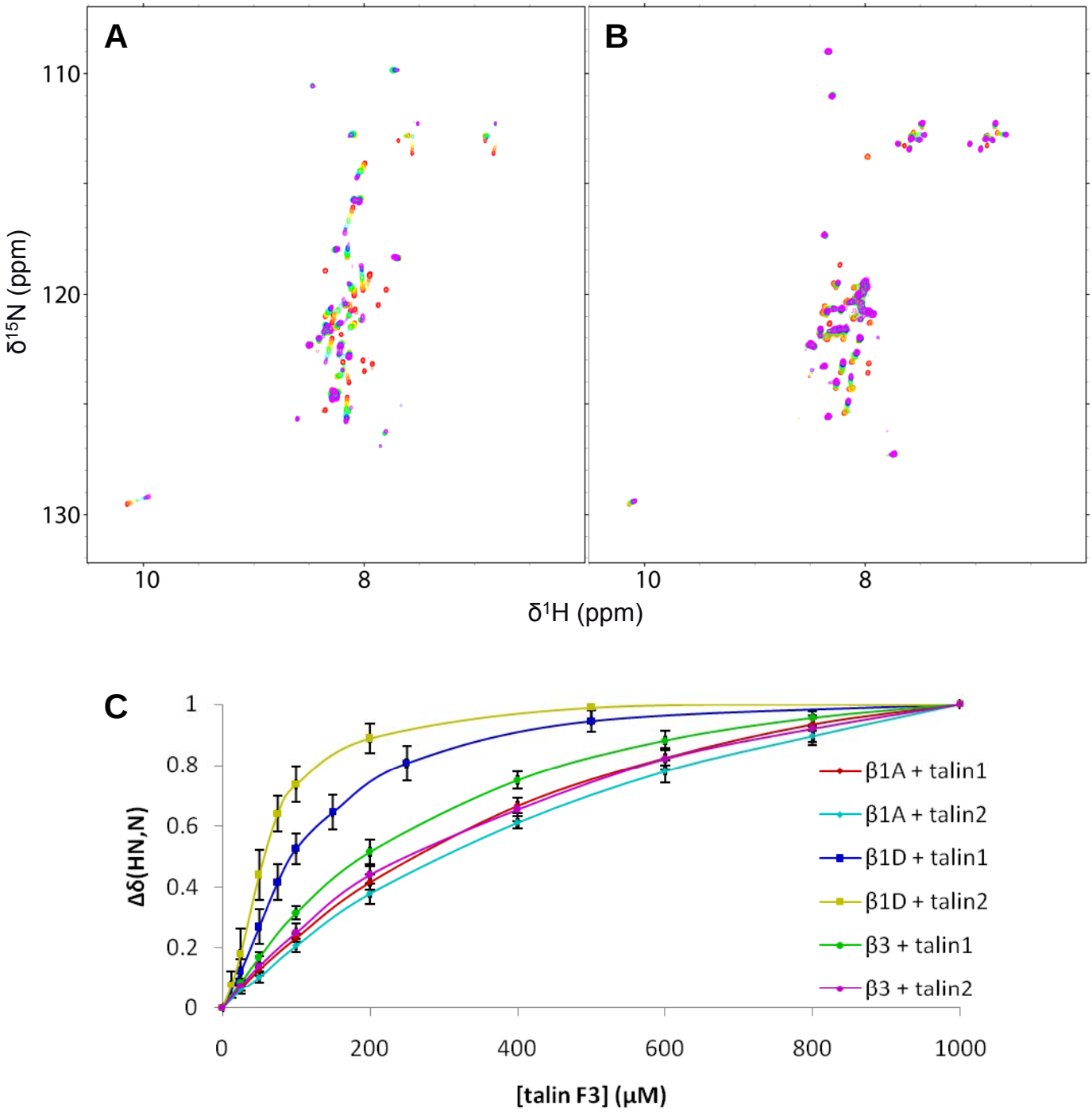

## Supplementary Figure S2

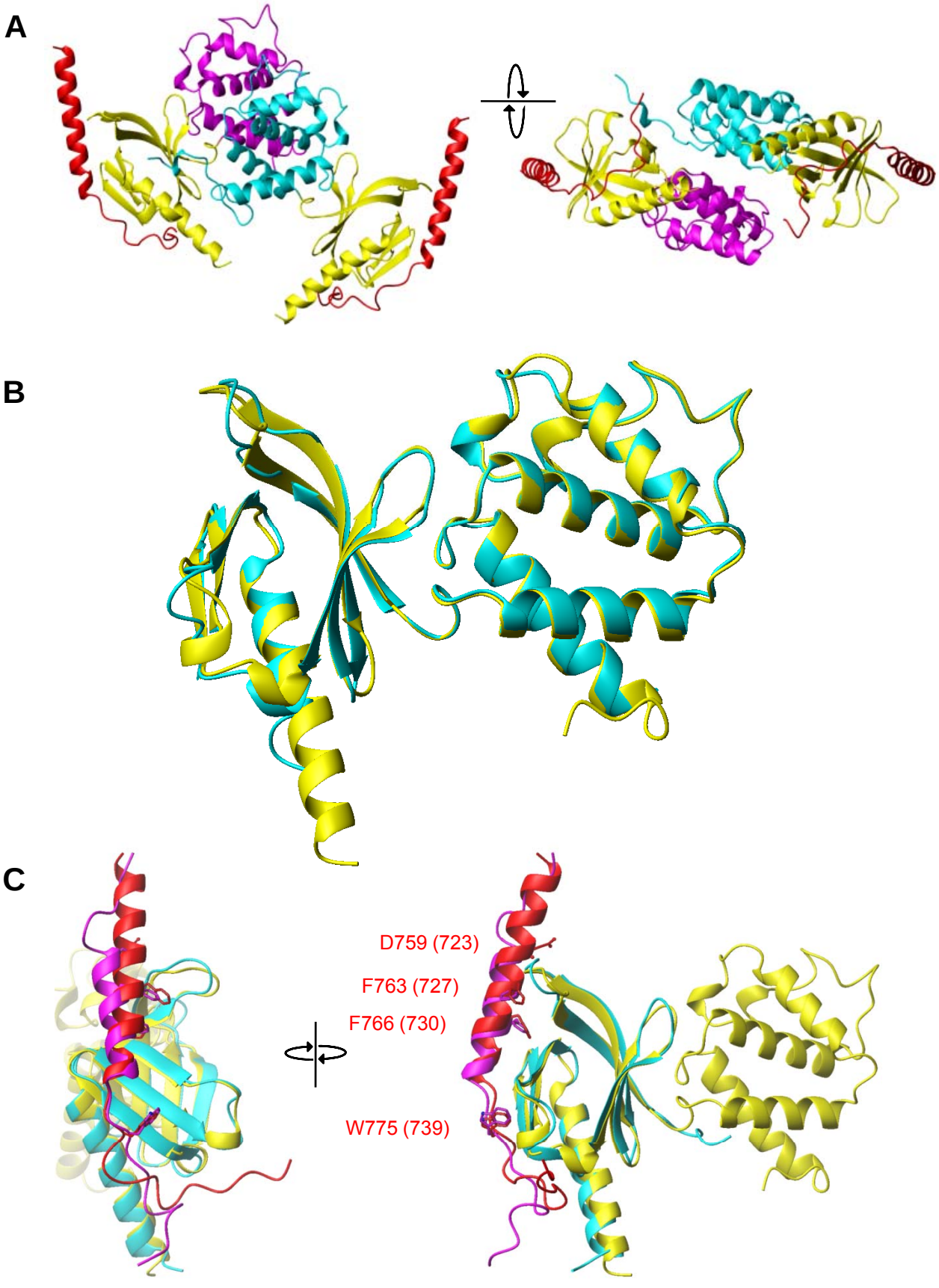

## Supplementary Figure S3

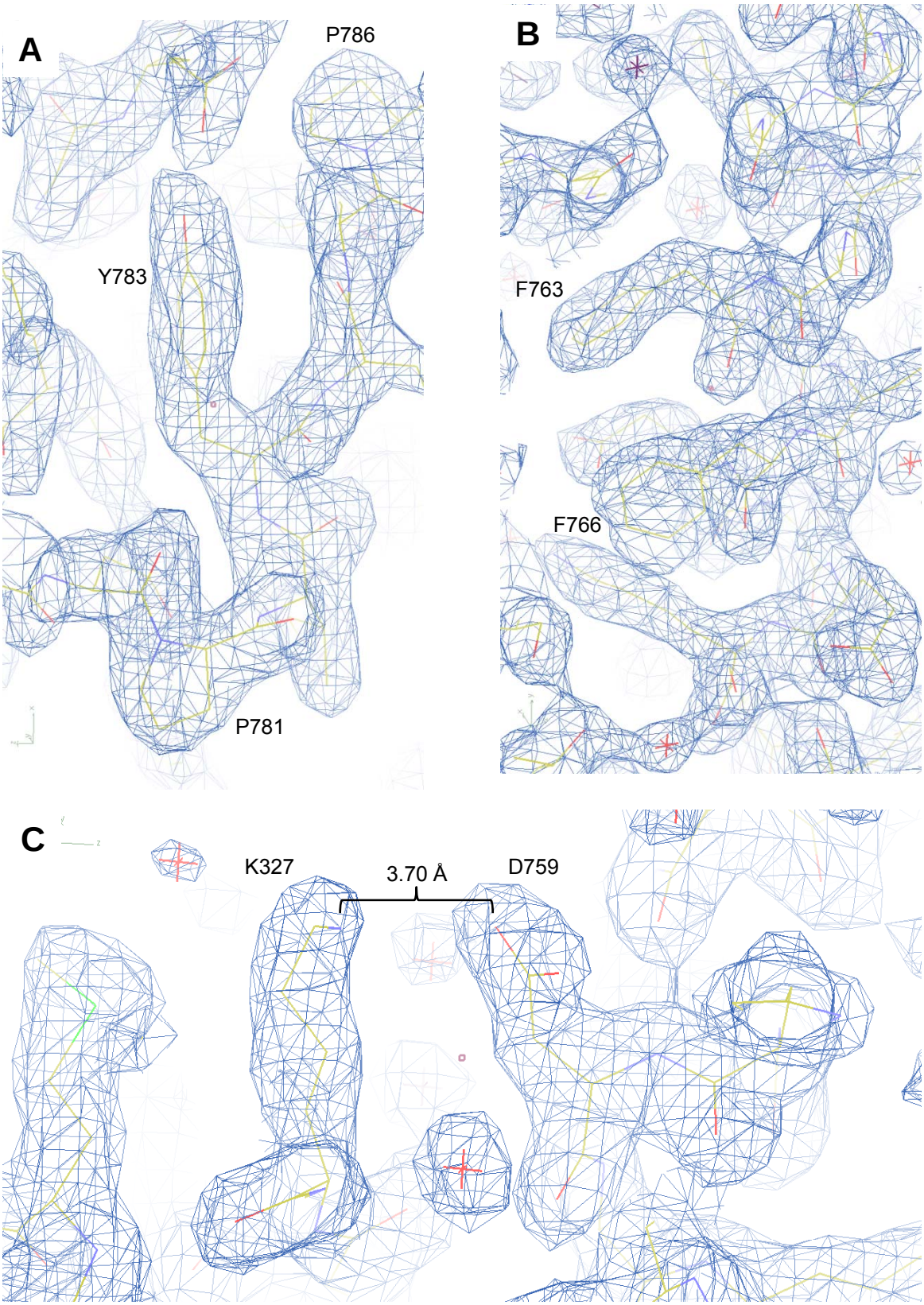

# Supplementary Figure S4

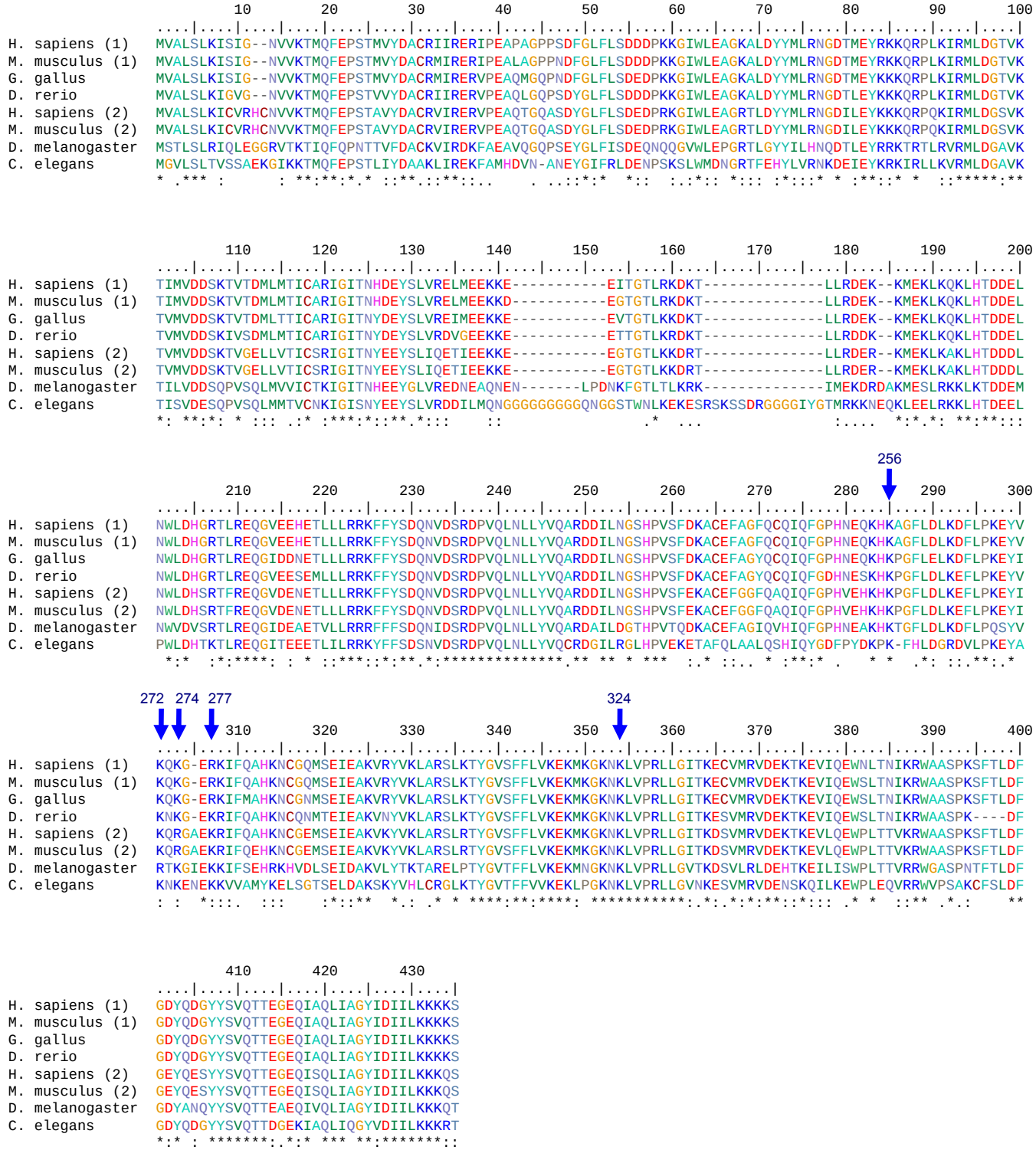

## Supplementary Figure S5

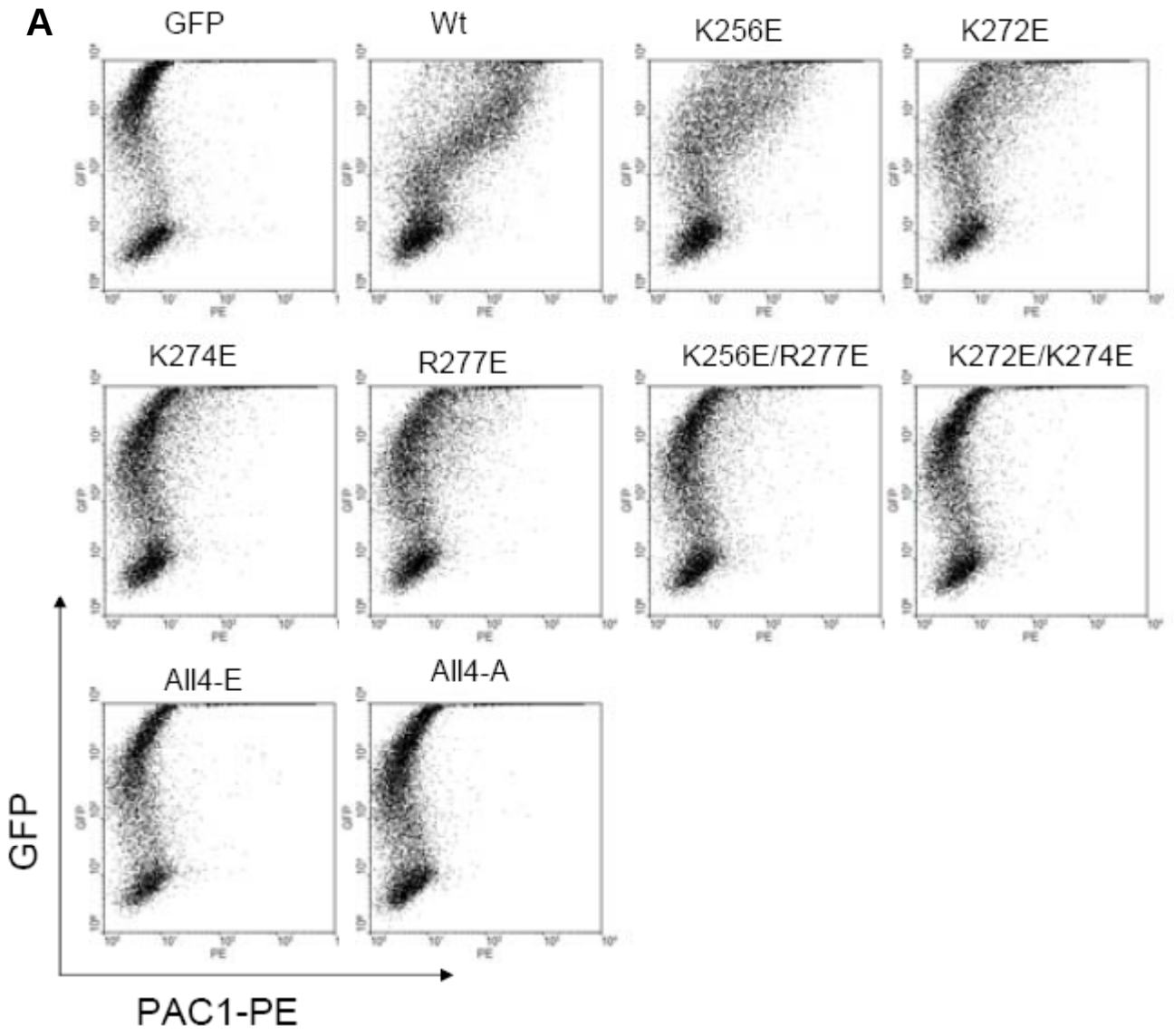


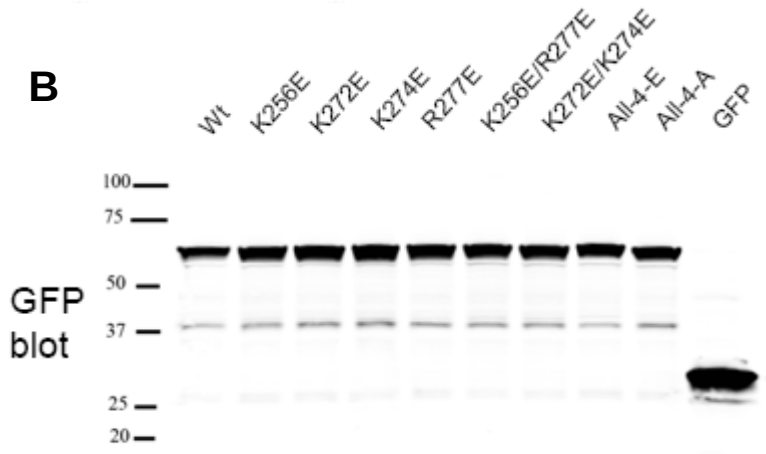

## Supplementary Figure S6

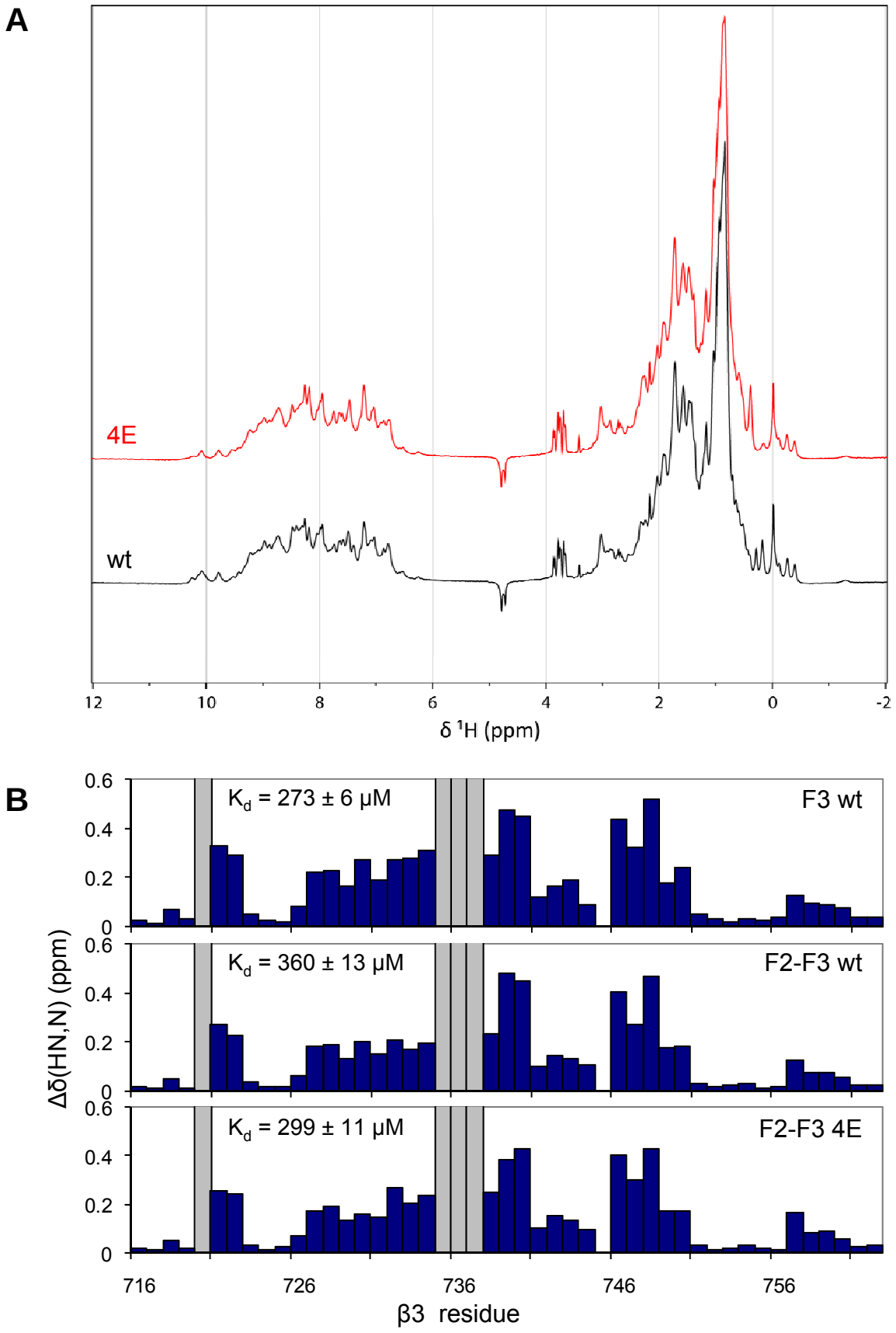

## Supplementary Figure S7

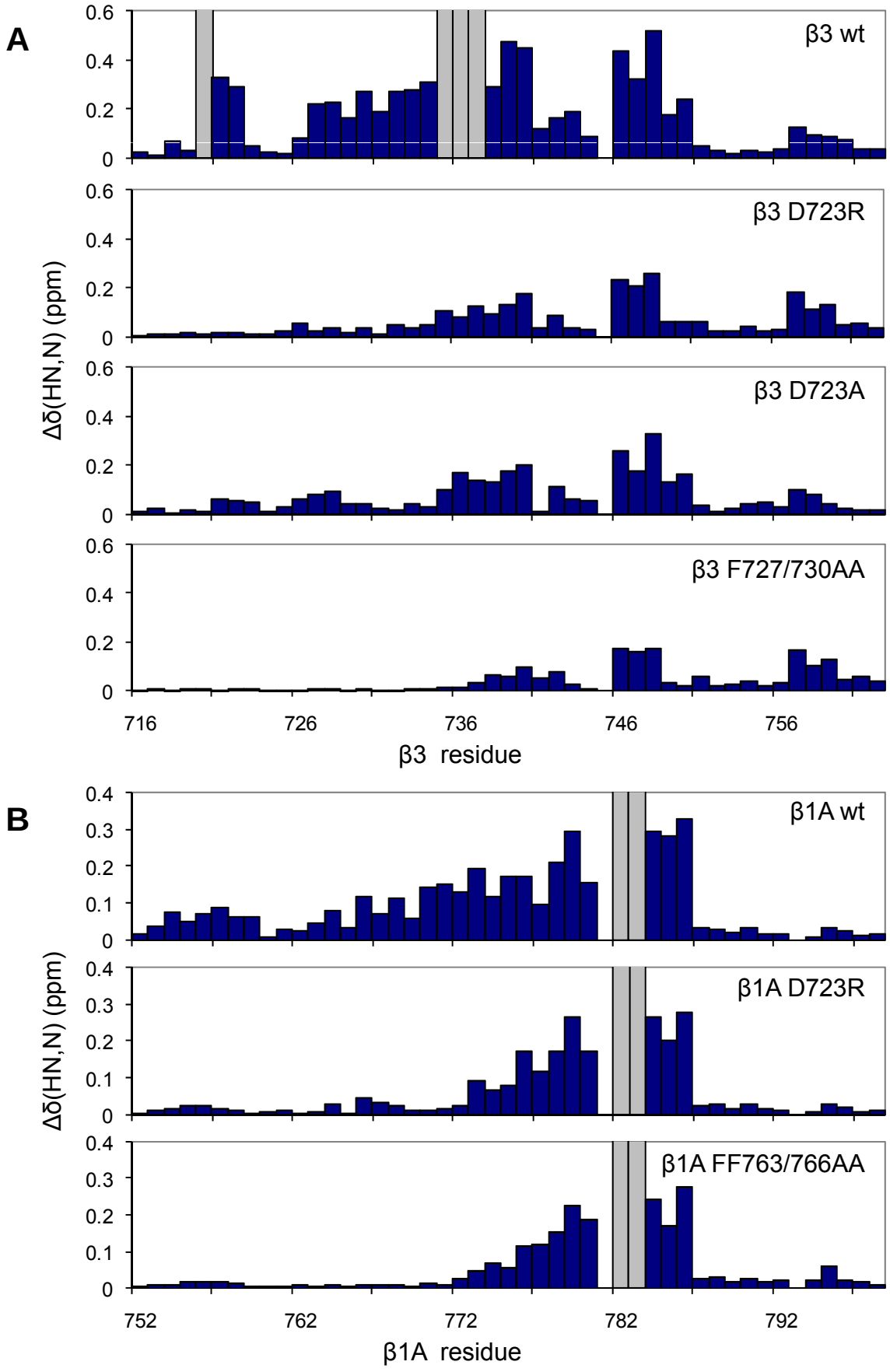

## Supplementary Figure S8